Int j simul model 24 (2025) 2, 297-308
Original scientific paper

SIMULATION AND OPTIMIZATION FOR OIL AND GAS PLATFORM PLACEMENT IN MOUNTAINOUS REGIONS

Dai, J. M.*; Zhu, H. M.**; Dai, Z. X.*; Chen, M.* & Du, L. B.**,#
* Research Institute of Natural Gas Gathering and Transmission Engineering Technology, PetroChina Southwest Oil and Gasfield Company, Chengdu, 610041, China
** School of Geoscience and Technology, Southwest Petroleum University, Chengdu, 610500, China
E-Mail: dulibing0622@126.com (# Corresponding author)

Abstract
Construction in mountainous regions involves substantial excavation and filling volumes. This study proposed an optimal location method for oil and gas platforms (OGPs) in mountainous regions. This method was based on multiple Particle Swarm Optimization (PSO). A geographic digital model was created for input elements such as residential areas, farmland, and roads. A total construction cost function was established, which incorporated excavation and filling costs, demolition compensation, and avoidance of key elements. A multiple PSO algorithm was developed to optimize platform location, corners, and elevation. This algorithm was validated using a real gas extraction platform. Results demonstrate that the geographic model accurately reflects surface features. The cost function has an error under 5 %, and it accurately represents location selection factors. The multiple PSO algorithm avoids local optima. Compared with actual location selections, the optimized solution reduces excavation by 40.4 %, filling by 35.3 %, and total costs by 27.3 %. This study provides a scientific basis for finding the optimal location for OGPs in mountainous areas.
(Received in March 2025, accepted in April 2025. This paper was with the authors 2 weeks for 2 revisions.)

Key Words: Oil and Gas Platforms, Mountainous Regions, Optimal Location, Cost Function, Multiple Particle Swarm Optimization

1. INTRODUCTION

OGPs are the direct platforms for oil and gas exploration and production. The construction costs of OGP are considerably affected by excavation and filling, boundary support, and land compensation in mountainous regions. OGPs need large-scale excavation and filling works. Excavation in mountainous areas rapidly disrupts the fragile balance of the original slope, which triggers geological disasters [1, 2]. Filling works are susceptible to causing uneven settlement disasters [3, 4]. High volumes of excavation and filling directly increase the cost of engineering treatment and also lead to a rise in boundary reinforcement costs. Meanwhile, the location of OGPs should meet the safety clearance requirements, such as situating it away from main pipelines, towns, and protected water sources. These restrictive conditions cause difficulty in selecting a suitable location for OGPs [5].

The impact of location on construction costs for OGPs in mountainous regions can exceed 75 % [6]. Reducing construction costs is a key objective in the location selection of OGPs in mountainous areas. However, traditional selection methods rely on the subjective designs of designers and software-based earthwork calculations. In addition, the final location requires rigorous verification, which typically takes over 15 days. Moreover, excessive excavation and backfill volumes may undermine the stability of OGPs. The traditional selection method for OGPs in mountainous regions depends on the designer's experience and has low precision, long duration, and high cost. At the same time, conventional optimization algorithms tend to converge to local optima and often produce non-unique solutions. A new optimal location selection method for OGPs in mountainous regions is needed to present terrain characteristics and construction costs, overcome solution non-uniqueness, and enhance location selection efficiency.

2. STATE OF THE ART

The location of OGPs affects early construction costs, long-term maintenance, and safety. The location selection should consider excavation volume, filling volume, demolition compensation, and avoidance distance of key elements. The conventional location selection method is subjective and cannot be considered comprehensively.

Currently, optimization has been successfully implemented across diverse application scenarios. For instance, Li et al. [7] applied an improved Gray Wolf Optimizer to distribution network optimization, which reduced total power losses by 25 %. Biswas et al. [8] decreased power losses by 12.7 % by employing the Black Widow Optimization algorithm. However, these methods were susceptible to local optima in complex optimization scenarios. An Adaptive Fuzzy Gray Wolf Optimizer was proposed by Sunil and Venkaiah [9], where fuzzy logic is integrated to manage uncertainties for avoiding local optima. Xi et al. [10] proposed a cooperative optimization approach with individual information exchange to improve the recycling rates of corrugated paper and avoid local optima. However, this methodology demonstrates instability when applied to large-scale facility location problems. Sharma et al. [11] used the Artificial Rabbit Optimization (ARO) algorithm in a 33-bus distribution network, but the ARO exhibited instability during iterations. Chen [12] developed an optimization algorithm to enhance route planning efficiency in distribution centres, which demonstrated superior global search ability. However, most conventional optimization algorithms are prone to local optima traps.

Unlike conventional optimization problems, location optimization must consider excavation and filling volume and demolition compensation. For instance, Ghazagh Jahed et al. [13] applied a water flow-inspired optimization algorithm to solve multi-objective power plant location problems. However, the accuracy of the solution was degraded during the objective-space transformation. Mohamed et al. [14] implemented a Tuna Swarm Optimization algorithm to handle complex optimal constraints. However, the multiple modelling assumptions may lead to substantial deviations. Wang et al. [15] proposed a hybrid multi-objective PSO algorithm, which has limited generalizability and adaptability. Farhan et al. [16] formulated a log-normal distributed parametric model, where the empirical cost parameters violated the assumed independent and identically distributed conditions. Doderovic et al. [17] integrated genetic algorithms with the Analytic Hierarchy Process to optimize waste rock dump layouts. However, the practical implementation of the model presented limitations in comprehensive factor inclusion. Raouti et al. [18] constructed a multi-variable optimization model with genetic algorithms to optimize wind farms. However, the location of wind farms did not focus on the high construction and maintenance costs. Zhu et al. [19] conducted location selection work for a logistics centre by optimizing logistics costs. However, the distribution of location selection parameters was complex in practice. Niu et al. [20] presented a decision tree-guided multi-objective evolutionary algorithm. However, the scalability of the model might be restricted. The effectiveness of optimization depended on verifying parameters in specific engineering cases.

In summary, existing studies mainly focus on layout optimization and path planning, with few works considering unavoidable earthwork and compensation. The cost functions could not reflect the actual characteristics of that in mountainous areas. The normal algorithms have difficulty avoiding local optima traps. This study proposed a new optimal location selection method for OGPs in mountainous areas. First, the new method found a digital geographic model that accurately characterizes constraints in mountainous regions. Secondly, it constructed a cost function considering earthwork volumes, reinforcement structures, and compensation factors. Finally, it proposed a multiple PSO algorithm for optimal location selection. The proposed method optimizes excavation and backfills volumes, reduces reinforcement and compensation costs, improves location selection efficiency, and offers a scientific reference for location selection for OGPs in mountainous regions.

The remainder of the study is organized as follows. Section 3 describes the entire process of optimal location selection for OGPs in mountainous regions, including the digital geographic model, the optimization functions, and multiple PSO algorithms for location selection. Section 4 takes an actual project as an example in verifying the application of the proposed location selection method. Section 5 summarizes the study and presents the relevant conclusions.

3. METHODOLOGY

3.1 Digital geographic model

Three-dimensional (3D) topographic elevation data critically affect the volume of excavation and backfill, as well as the area of pre-existing infrastructure (roads, buildings, farmland). Therefore, a geospatial modelling system is essential. This study obtains terrain point cloud data through UAV LiDAR in the potential zone. The "griddata" mesh interpolation function in MATLAB is then used to create a terrain mesh surface. Subsequently, key elements such as roads, residential areas, rivers, and farmlands are input and managed using DXF format files in CAD. Based on layer numbering, this study establishes rules for inputting and modelling key elements between CAD and MATLAB. The implementation of the digital geographic model follows these steps:

The mesh grid function in MATLAB was employed to set the grid size (L_x) and generate grid data. This product served as the digital foundation. In general, when the mesh sizes (L_x) are smaller, the accuracy of the terrain surface is higher, but more computational resources are required. A grid size of L_x = 0.5 m was recommended when considering actual computational resources.

As shown in Fig. 1, the key elements (e.g., residential buildings, roads, and ponds) were obtained through UAV aerial photography. The contours of key elements were extracted using ArcGIS software. Subsequently, field investigations were conducted to refine the height and depth information of key elements. Geometric information for the concealed key elements (e.g., mineral rights and culverts) was supplemented. A measurement CAD file was generated based on the above-mentioned procedures.

Figure 1: Key element identification from aerial imagery.

The key elements are categorized into three types: topographic elements, demolishable elements, and avoidance elements. Topographic elements record terrain data. Demolishable elements mainly include residential buildings, roads, and ponds. Avoidance elements primarily encompass schools, expressways, and water sources. The key elements were categorized into layers in CAD according to topographic, demolishable, and avoidance elements. The elements were exported as a DXF file and imported into MATLAB. Table I shows the input rules for key elements, where numbers represent spatial information. For example, the number for residential buildings indicates the number of floors. The road number minus 21 implies width. The pond number minus 41 represents silt depth. These layer numbers enable the generation of spatial 3D key elements.

Table I: Location selection elements.

Type	Element	Number	Notes
Topographic Elements	Terrain Point Cloud	0	Terrain Point Cloud
Demolishable Elements	Residential Buildings	1-20	Building Area
	Roads	21-40	Road Class
	Ponds	41-60	Area and Location
	Farmland	61-70	Area and Location
Avoidance Elements	Schools, Hospitals, Large Oil Depots	101	Avoidance Level 1 Distance of 500 m
	High-Voltage Power Lines	102	
	High-Speed Railways	103	Avoidance Level 2 Distance of 200 m
	Expressways	104	
	Protected Water Sources	105	
	Mineral Rights	106	Avoidance Level 3, Distance of 0 m
	Permanent Farmland	107	

Smaller grid sizes resulted in more grid cells, but computation times became longer. Assuming that the height of a single-story residential building is 3 m, the residential building can be drawn based on the number of floors. Meanwhile, the road can be calculated based on its centreline and width. The final regional terrain information model is shown in Fig. 2.

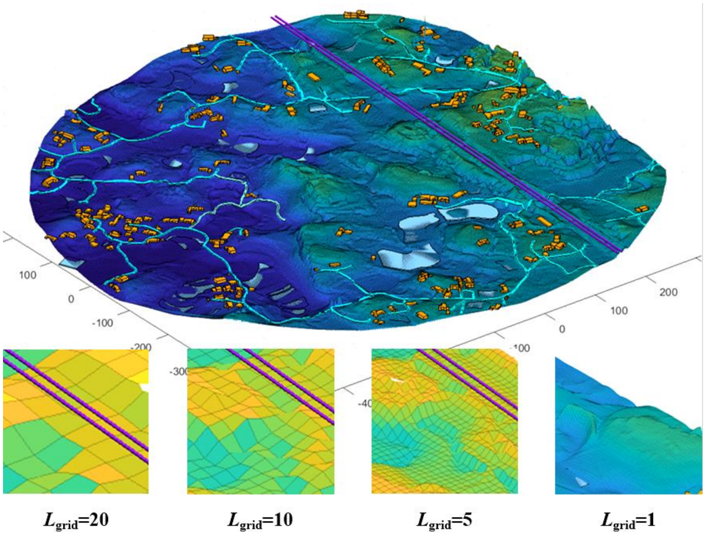

Figure 2: Geographic model with different grid sizes.

3.2 Cost function for oil and gas station construction

The optimization variables included the location (S_x, S_y), rotation angle α, and elevation h for OGPs in mountainous regions. The volume of excavation and backfill was calculated using a 3D terrain mesh. A cost function was constructed, which included excavation and filling, slope reinforcement, and demolition compensation. The centre point S (S_x, S_y) of OGP must not exceed the potential selection regions ($x \in$ [min(x), max(x)], $y \in$ [min(y), max(y)]). It must be situated away from non-demolishable buildings, high-speed railways, expressways, and permanent farmland. According to different protection levels i, all points (K_{xi}, K_{yi}) of the avoidance element must maintain a safety distance from the OGP. The OGP rotation angle $\alpha \in [0°, 180°]$.

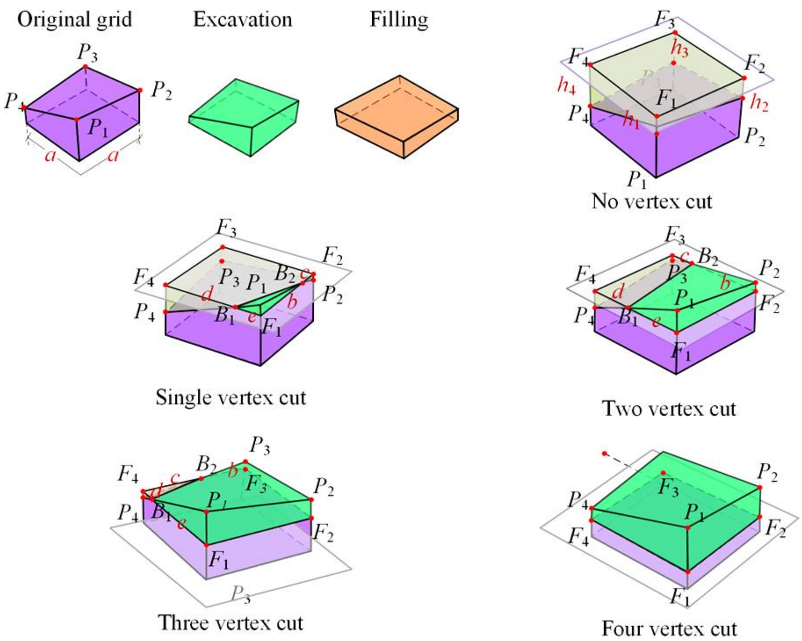

Figure 3: Excavation and filling volumes for different cutting conditions.

The excavation and filling volumes were the key to the cost function. The actual 3D terrain was composed of several basic units of terrain mesh. Each mesh was a square planar projection with a side length of L_{gird}. The portion lying above the construction plane was considered excavation, while the portion below was regarded as filling. As shown in Fig. 3, the terrain vertices are P_1, P_2, P_3, and P_4, which are arranged counterclockwise. Each vertex may have different elevations. The vertical projections of the terrain vertices P_1, P_2, P_3, and P_4 onto the construction plane are F_1, F_2, F_3, and F_4, respectively. The elevation differences between the projection points and the terrain vertices are h_1, h_2, h_3, and h_4. The relative position between the terrain mesh unit and the construction plane can be classified into five cases: no vertex cut, single-vertex cut, two-vertex cut, three-vertex cut, and four-vertex cut. When a single-vertex cut, a two-vertex cut, or a three-vertex cut was considered, the intersection points B_1 and B_2 between the construction plane and the edges of the terrain mesh were calculated. First, the most minor numbered cut point was numbered as 1, and the unit grid points were renumbered in a counterclockwise order. Then, following the counterclockwise order, the intersection point on the left side of node 1 is B_1, and that on the other side is B_2. The excavation and filling volumes were calculated, as shown in Fig. 3.

1) In the case with no vertex cut, all the elevation differences $h_i > 0$, where $i \in [1, 4]$. The numbering of the terrain grid vertices remained unchanged. The excavation and filling volumes within a single grid are given by Eq. (1):

$$\begin{cases} V_{E1} = 0 \\ V_{F1} = \dfrac{{L_{gird}}^2}{4}(h_1 + h_2 + h_3 + h_4) \end{cases} \tag{1}$$

2) When only a single-vertex cut was considered, one of the four elevation differences was less than zero. The vertex to be cut was numbered 1, and the remaining points were

renumbered in a counterclockwise order. The intersection point on the left side of node 1 is B_1, and that on the other side is B_2. The distances e between projection points F_1 and B_1 and b between F_1 and B_2 were then calculated. The excavation volume and the filling volume were calculated, as shown in Eq. (2):

$$\begin{cases} V_{E2} = \dfrac{beh_1}{6} \\ V_{F2} = ({L_{gird}}^2 - \dfrac{be}{2})\dfrac{h_2 + h_3 + h_4}{5} \end{cases} \tag{2}$$

3) Two elevation differences were less than zero when two vertexes were cut. The vertex with the smallest number among the cut vertices was numbered 1, and the unit grid points were renumbered in a counterclockwise order. The intersection point on the left side of node 1 is B_1, and that on the other side is B_2. The distances e between F_1 and B_1, d between F_4 and B_1, b between B_2 and the projection point closest to F_1, and c between B_2 and the farther projection point were then calculated. The excavation volume and the filling volume were calculated, as shown in Eq. (3):

$$\begin{cases} V_{E3} = \dfrac{L_{gird}}{8}(b+e)(h_1 + h_2) \\ V_{F3} = \dfrac{L_{gird}}{8}(c+d)(h_3 + h_4) \end{cases} \tag{3}$$

4) Three elevation differences were less than zero when three vertexes were cut. The vertex with the smallest number among the cut vertices was numbered 1, and the unit grid points were renumbered in a counterclockwise order. The intersection point on the left side of node 1 is B_1, and that on the other side is B_2. The distance d between projection points F_4 and B_1 and c between projection points F_4 and B_2 were then calculated. The excavation volume and the filling volume were calculated, as shown in Eq. (4):

$$\begin{cases} V_{E4} = ({L_{gird}}^2 - \dfrac{cd}{2})\dfrac{h_1 + h_2 + h_3}{5} \\ V_{F4} = \dfrac{cdh_4}{6} \end{cases} \tag{4}$$

5) Four elevation differences less than zero when four vertexes were cut. Eq. (5) calculates the filling volume:

$$\begin{cases} V_{E5} = \dfrac{{L_{gird}}^2}{4}(h_1 + h_2 + h_3 + h_4) \\ V_{F5} = 0 \end{cases} \tag{5}$$

The terrain grids were classified into five cases: no vertex cut, single-vertex cut, two-vertex cut, three-vertex cut, and four-vertex cut. The excavation and fill volumes of each grid were then calculated using Eqs. (1) to (5). The final excavation and fill volume are calculated by Eq. (6):

$$\begin{cases} V_E = \sum V_{E1} + \sum V_{E2} + \sum V_{E3} + \sum V_{E4} + \sum V_{E5} \\ V_F = \sum V_{F1} + \sum V_{F2} + \sum V_{F3} + \sum V_{F4} + \sum V_{F5} \end{cases} \tag{6}$$

If the excavation and filling volumes are not balanced, then additional costs for soil disposal will be incurred. If the excavation volume exceeds the filling volume, then extra space is needed to store surplus soil and rock. Conversely, if the filling volume exceeds that of excavation, then more soil and rock must be excavated to meet the filling requirements:

$$V_T = V_E - V_F \tag{7}$$

The construction plane is a sloping surface when the slope grading with a certain inclination angle is implemented around OGPs. For simplification, the slope surface was discretized into multiple discontinuous horizontal planes with different elevations. During the filling process, if the depth of the filling area reaches 2 m, then a retaining wall is constructed to maintain the stability. The length of the retaining wall can be calculated by the centres of the grids. The new road was simplified to the nearest straight line from the centre of OGP to the existing road. In addition, the centre of the OGP should remain a certain distance from the boundary. In this study, the boundary distance L_{void} = 50 m. The total construction cost of OGPs was combined with the excavation volume, the filling volume, the length of the retaining wall L_W, the length of the new road L_R, and the demolition areas A_D, as shown in Eq. (8):

$$\begin{gathered} f(S_x, S_y, S_\alpha, S_h) = V_E P_E + V_F P_F + V_T P_T + L_W \cdot P_W \\ + L_R \cdot P_R + \sum_{i=1}^{n} A_{Di} \cdot P_{Di} \\ \begin{cases} P_T = \begin{cases} P_E & V_T > 0 \\ P_T & V_T < 0 \end{cases} \\ x_{\min} + 50 < S_x < x_{\max} - 50 \\ y_{\min} + 50 < S_y < y_{\max} - 50 \end{cases} \end{gathered} \tag{8}$$

In Eq. (8), P represents the cost quotas for various items. For example, P_E is the excavation quota per unit volume, P_F is the filling quota per unit volume, P_T is the earthwork transportation quota per unit volume, P_W is the retaining wall construction quota per unit length, P_R is the quota for constructing a new road per unit length, and P_R is the compensation quota per unit area for different elements. P_{Di} includes residential buildings, ponds, farmlands, bamboo groves, and other types. The cost quota parameters are derived from actual OGP.

3.3 Multiple particle swarm optimization for location selection

The normal PSO algorithm is inspired by the cooperative foraging behaviour of bird flocks. Each "particle" represents a candidate solution in the solution space. By tracking its historical optimal position and the global optimal position of the swarm, each particle dynamically adjusts its velocity and position. A swarm of particles (with positions and velocities) is randomly generated. Subsequently, based on the objective function, the algorithm records the local best optimum and the global best optimal value. Finally, the position is updated. Let $v(t)$ and $x(t)$ represent the current velocity and position of a particle, respectively, while $v(t+1)$ and $x(t+1)$ denote the updated velocity and position. r_1 and r_2 are random numbers between [0, 1], which introduce randomness in particle movement. The inertia weight is denoted by w, and c_1 and c_2 are acceleration factors. The algorithm outputs the result when the maximum number of iterations is reached or the convergence threshold is met:

$$v_{ij}(t+1) = v_{ij}(t) + c_1 r_1(t)\left[p_{ij}(t) - x_{ij}(t)\right] + c_2 r_2(t)\left[p_{gj}(t) - x_{ij}(t)\right] \tag{9}$$

$$x_{ij}(t+1) = x_{ij}(t) + v_{ij}(t+1) \tag{10}$$

A single optimization can generate different results for the same problem. This study proposed a new method called the multiple PSO algorithms to find the optimal location for OGPs. The multiple PSO algorithms performed repeated and independent optimizations. The best solution was selected from the numerous optimal results. The proposed method provided a unique optimal location of OGPs in mountainous regions. The multiple PSO algorithm first repeated *m* independent PSO runs under the same optimization conditions, which produced *m* initial optimal locations. Subsequently, these optimal locations were statistically analysed to identify a final optimal location.

By increasing the number of optimization times, the results from various PSO algorithms effectively cover the global optimal solution. This approach should effectively avoid multiple solutions. A critical optimal number of N_{cr} exists. To determine this critical number N_{cr} for multiple PSO algorithms, optimization runs were performed with 5, 10, 20, 25, 50, and 100 runs.

The shape of the OGP in mountainous regions was simplified to a rectangle. The location of the OGP was optimized to minimize construction costs while meeting the necessary constraints and requirements. First, constraints were set according to the avoidance requirements, and an initial location of OGP was randomly generated. Subsequently, the total construction cost of the OGP in the mountainous region was calculated according to the objective function. Multiple PSO runs were performed, which recorded the local and global optimal results for the optimal location selection. Finally, the optimal location was updated.

The location information (OGP coordinates ($x_{optimal}$, $y_{optimal}$), OGP angle $\alpha_{optimal}$, and OGP elevation $H_{optimal}$), cost information (e. g., total construction cost, demolition cost, and road cost), and earthwork details (e. g., excavation volume, filling volume, and reinforcement length) were output to provide a basis for subsequent design.

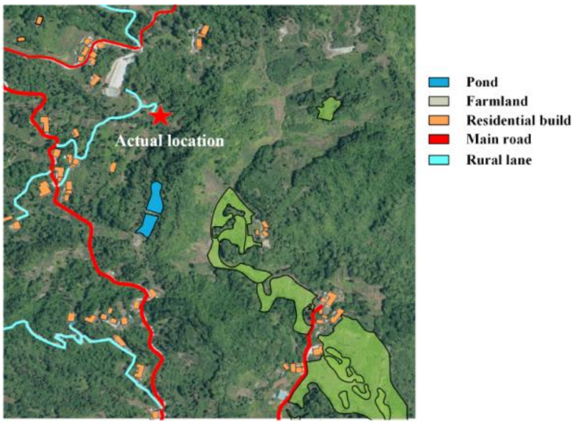

Figure 4: Aerial imagery.

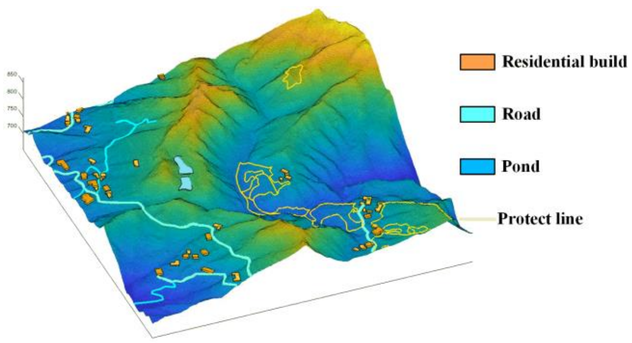

Figure 5: Digital geographic model.

4. CASE STUDY

4.1 Overview of the potential area in mountainous regions

An OGP was situated in the mountainous area of Ziyang City, Sichuan Province. The 3D terrain of the selection area is shown in Fig. 4. The selection area is a square with a side length of 800 m. The shape of the OGP measured 108 m × 55 m. The west of the selection area encompassed roads, residential buildings, and ponds. The south held an extensive permanent farmland. The north and west sides featured significant terrain undulations. The construction of the OGP encountered extensive excavation and filling volumes and severe geological risks. This case study was used to evaluate the effectiveness of the proposed method.

4.2 Digital geographic model

The CAD data provided information on residential buildings, roads, ponds, high-speed railways, expressways, and other elements. Following the established rules, each key element is saved in the corresponding layer. The interpolation processing is performed with a grid side length of L_{grid} = 0.5 m. As shown in Fig. 5, the relatively flat areas are densely covered by farmland protection red lines, which significantly restrict and compress the available space for station location selection. Consequently, optimization becomes crucial to reduce earthwork volumes, minimize demolition compensation, and avoid protected red lines.

4.3 Determination of parameters for the cost function

The volumes of excavation and filling were calculated based on the actual location of the OGP to verify the feasibility of the proposed method. The comparison is shown in Table II. The error of the excavation volume shows a difference of 1.5 %, and the error of the filling volume exhibits a difference of 4.9 %. This result verifies the reliability of the excavation and filling volumes derived from the cost function and digital geographic model.

Table II: Comparison with actual and calculated earthwork for the OGP at Ziyang City.

Parameter	Actual volume	Calculated volume	Unit	Error
Filling	38,465.16	39,062.93	m^3	1.5 %
Excavation	32,925.15	31,379.84	m^3	4.9 %

The quota parameters are input as shown in Table III. It considers the costs of excavation and filling, boundary retaining walls, and land compensation. In this case study, the quota parameters were from the completed construction projects of the OGP in mountainous regions, Ziyang City, Sichuan Province.

Table III: Parameters for the OGP in mountainous regions, Ziyang City, Sichuan Province.

Name	Parameter	Input value	Unit
Cost Quotas	Excavation	27.49	¥/m^3
	Filling	7.82	¥/m^3
	Surplus Soil Transportation	5.64	¥/m^3
	Boundary Retaining Wall	734.09	¥/m
	Road Construction	1,732.29	¥/m
	Residential Compensation	900	¥/m^2
	Farmland Compensation	42	¥/m^2
	Pond Compensation	89.5	¥/m^2

5. RESULT ANALYSIS AND DISCUSSION

5.1 Critical number of multiple PSO

Theoretically, increasing the optimization times leads to a more stable optimal solution. Statistical results of the optimal solutions at different times of multiple PSOs are shown in Table IV. As indicated in Table IV, the critical number of optimization N_{cr} = 25. The planar distribution of the optimal location under different optimization times is depicted in Fig. 6 a. As shown in the figure, when the number of optimizations is low, the optimal OGP occupies more residential buildings and ponds. It also intersects with existing roads, which leads to additional fees for new road construction.

Table IV: Statistics of multiple deep optimization results.

Number	Total Cost (¥)	Filling (m^3)	Excavation (m^3)
5	1,338,091	37,885	38,033
10	1,291,409	34,962	33,080
15	1,039,614	33,710	32,197
20	992,896	23,508	22,574
25	853,642	25,099	24,118
100	847,146	24,869	23,929

5.2 Optimal results from multiple PSO

Fig. 6 b shows the final optimal location, which is close to the existing road, and no residential demolition compensation. The final optimization result is compared with the actual station cost in Table V. As shown in Table V, the optimal location for the OGP in the mountainous region results in a 40.4 % reduction in total costs, a 35.3 % decrease in excavation volume, and a 27.3 % decline in filling volume compared with the results from manual methods. The proposed method effectively reduces the cost of the OGP in the mountainous region.

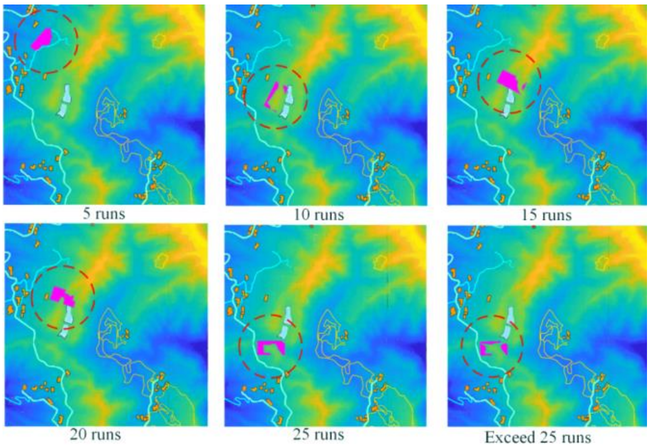

a) location generated by different optimal numbers

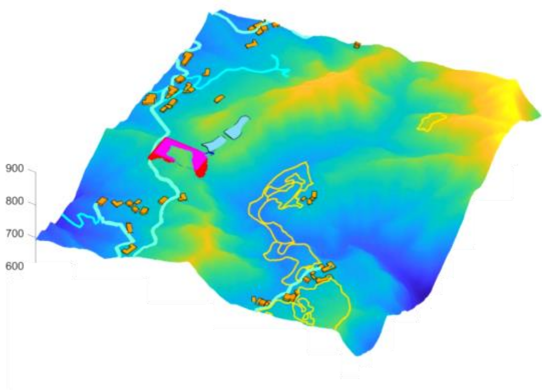

b) final location

Figure 6: Optimal location generated by multiple optimization.

Table V: Detailed results of the comparison between the optimal cost and the actual cost.

Name	Optimal value	Actual value	Unit
Total Cost	847,146	1,423,531	¥
Filling Volume	24,869	38,465	m^3
Excavation Volume	23,929	32,925	m^3
Road Construction Cost	7070	275,632	¥
Residential Demolition Area	0.00	569	m^2

6. CONCLUSION

This study proposed a new location selection method to quantify construction costs and identify the optimal location for OGPs in mountainous regions. The technique first established a digital geographic model, constructed a cost function and employed a multiple PSO algorithm to find the optimal location in mountainous regions. The following conclusions could be drawn:

(1) The combination of MATLAB-CAD creates a geographic model that accurately reflects the 3D undulating terrain and key features. The generated geographic model provided a solid data foundation for the location selection of OGPs in the mountainous region.

(2) The construction cost included earthwork volume, compensation, and road construction costs. Practical applications have shown that the workload calculated by the proposed cost function deviates by less than 5 % from the actual workload.

(3) Numerical experiments indicate that, after 25 optimization runs, the optimal solution stabilizes and is unique. Compared with the actual location, the optimized cost of excavation and filling is reduced by 40.4 %, the excavation volume is decreased by 35.3 %, and the filling volume is lessened by 27.3 %.

This study proposes a location selection method for OGPs in mountainous regions, which can reduce earthwork volumes and construction costs. It provides a scientific reference for the location selection of OGPs in mountainous regions. The shape in this study was simplified to a standard rectangle. Therefore, future research will focus on optimizing the irregular shape of OGPs.

REFERENCES

[1] Qin, H.; Yin, X.-T.; Tang, H.; Xu, C. (2024). Design method for active slope reinforcement: a case study of excavated slopes (in Chinese), *Coal Geology & Exploration*, Vol. 52, No. 11, 86-95, doi:10.12363/issn.1001-1986.24.04.0258

[2] Duan, R.; Tang, R.; Wang, Z.; Yang, J.; Su, J. (2023). Optimized layout of supporting facilities in mountainous industrial parks: a case study of Chongqing Dadi Industrial Park, *Frontiers in Ecology and Evolution*, Vol. 11, Paper 1243778, 10 pages, doi:10.3389/fevo.2023.1243778

[3] Zhao, J.-J.; Xie, M.-L.; Yu, J.-L.; Chai, H.-J.; Li, T.; Zhao, W.-H. (2017). Experimental study on the deformation and failure mechanism of fill slope induced by engineering load, *Journal of Engineering Geology*, Vol. 27, No. 2, 426-436, doi:10.13544/j.cnki.jeg.2017-368

[4] Kamagawa, H.; Xu, Q.; Zhao, K.-Y.; Jiang, Y.-N.; Guo, P.; Du, P.-C.; Yuan, S. (2020). Research on land subsidence and vegetation restoration characteristics of Pingshan city-building project in Yan'an New Area based on remote sensing analysis (in Chinese), *Journal of Engineering Geology*, Vol. 28, No. 3, 597-609, doi:10.13544/j.cnki.jeg.2019-107

[5] Liang, X.; Shan, C.-A.; Zhang, L.; Luo, Y.-F.; Jiang, L.-W.; Wang, G.-C.; Li, B.-S.; Zhang, R.-J.; Li, L.-J.; Wang, X. (2023). Exploration and development progresses and resource potentials of multi-type unconventional gas reservoirs characterized by in-source reservoir and accumulation in complex tectonic areas of Southern China (In Chinese), *Acta Petrolei Sinica*, Vol. 44, No. 12, 2179-2199, doi:10.7623/syxb202312011

[6] Wang, Y.-Z.; Luo, J.; Guo, R.-Y.; Li, Y.-D. (2015). Pre-drilling engineering cost management in the background of two new laws (in Chinese), *Natural Gas Industry*, Vol. 35, No. 9, 123-126

[7] Li, P.; Dong, H.-N.; Zhang, G.-F.; Bai, X.; Zhao, X. (2023). Research on loss reduction strategy of distribution network based on distributed generation site selection and capacity, *Energy Reports*, Vol. 9, Suppl. 8, 1001-1012, doi:10.1016/j.egyr.2023.05.045

[8] Biswas, P. P.; Mallipeddi, R.; Suganthan, P. N.; Amaratunga, G. A. J. (2017). A multiobjective approach for optimal placement and sizing of distributed generators and capacitors in distribution network, *Applied Soft Computing*, Vol. 60, 268-280, doi:10.1016/j.asoc.2017.07.004

[9] Sunil, A.; Venkaiah, C. (2024). Multi-objective Adaptive Fuzzy Campus Placement based Optimization Algorithm for optimal integration of DERs and DSTATCOMs, *Journal of Energy Storage*, Vol. 75, Paper 109682, 16 pages, doi:10.1016/j.est.2023.109682

[10] Xi, Y.-L.; Tao, F.-M.; Brooks, S. (2023). Optimization of carton recycling site selection using particle swarm optimization algorithm considering residents' recycling willingness, *PeerJ Computer Science*, Vol. 9, Paper 1519, 23 pages, doi:10.7717/peerj-cs.1519

[11] Sharma, R. K.; Naick, B. K. (2024). A novel Artificial Rabbits Optimization algorithm for optimal location and sizing of multiple distributed generation in radial distribution systems, *Arabian Journal for Science and Engineering*, Vol. 49, No. 5, 6981-7012, doi:10.1007/s13369-023-08559-1

[12] Chen, X.-J. (2024). Location strategy for logistics distribution centers utilizing improved whale optimization algorithm, *Journal of Intelligent Systems*, Vol. 33, No. 1, Paper 20230299, 13 pages, doi:10.1515/jisys-2023-0299

[13] Ghazagh Jahed, Y.; Mousazadeh Mousavi, S. Y.; Golestan, S. (2024). Optimal sizing and siting of distributed generation systems incorporating reactive power tariffs via water flow optimization, *Electric Power Systems Research*, Vol. 231, Paper 110278, 12 pages, doi:10.1016/j.epsr.2024.110278

[14] Mohamed, A. A.; Kamel, S.; Hassan, M. H.; Kamalov, F.; Safaraliev, M. (2024). Optimizing FACTS devices location and sizing in integrated wind power networks using Tuna Swarm Optimization algorithm, *Journal of Thermal Analysis and Calorimetry*, Vol. 149, No. 13, 7135-7153, doi:10.1007/s10973-024-12909-y

[15] Wang, Y., Wang X.-W.; Wei, Y.-H.; Sun, Y.-Y.; Fan, J.-X.; Wang, H.-Z. (2023). Two-echelon multi-depot multi-period location-routing problem with pickup and delivery, *Computers & Industrial Engineering*, Vol. 182, Paper .109385, 29 pages, doi:10.1016/j.cie.2023.109385

[16] Farhan, M.; Schneider, R.; Thöns, S.; Gündel, M. (2025). Probabilistic cost modeling as a basis for optimizing inspection and maintenance of turbine support structures in offshore wind farms, *Wind Energy Science*, Vol. 10, No. 2, 461-481, doi:10.5194/wes-10-461-2025

[17] Doderovic, A.; Doderovic, S.-M.; Stepanovic, S.; Bankovic, M.; Stevanovic, D. (2023). Hybrid model for optimisation of waste dump design and site selection in open pit mining, *Minerals*, Vol. 13, No. 11, Paper 1401, 22 pages, doi:10.3390/min13111401

[18] Raouti, D.; Bouanane, A.; Tahtah, A.; Meziane, R.; Vido, L.; Touhami, S. (2025). LCOE optimization of a wind farm according to the transport and installation phase and unit power, *Iranian Journal of Science and Technology, Transactions of Electrical Engineering*, Vol. 49, No. 2, 711-723, doi:10.1007/s40998-025-00789-3

[19] Zhu, Y.; Fan, X.; Yin, C. (2024). Aptenodytes forsteri optimization algorithm for low-carbon logistics network under demand uncertainty, *PLoS ONE*, Vol. 19, No. 1, Paper 0297223, 28 pages, doi:10.1371/journal.pone.0297223

[20] Niu, Y.; Xu, C.; Liao, S.; Zhang, S.; Xiao, J. (2024). Multi-objective location-routing optimization based on machine learning for green municipal waste management, *Waste Management*, Vol. 181, 157-167. doi:10.1016/j.wasman.2024.04.001